DoA Estimation with a Single Antenna and a Few Low-Cost Backscattering Tags

Georgios Vougioukas and Aggelos Bletsas *Senior Member, IEEE*

Abstract

Backscatter radio utilizes the reflection that an electromagnetic wave undergoes when it impinges an unmatched-to-a-load antenna, in order to achieve ultra-low-power communication. This work exploits principles commonly found in the ultra-low-power, backscatter communication literature, offering multi-element array functionalities to a single-antenna receiver. A small number of simple, switching backscattering tags deployed in space, emulate a distributed, multi-element antenna array by copying a transmitter's signal to distinct frequency bands. A receiver can then obtain independent observations of the same signal by discriminating said bands. Using the backscatter tag-based array, the direction of arrival (DoA) estimation problem is addressed without the cost of multiple RF front ends or hardware modifications, at either end of a wireless communication link. The feasibility of the idea was examined through both simulations and experimental deployments. An absolute error of ≈ 20 degrees was observed when utilizing 5 custom-built backscattering tags, while simulations showed that more than 10 tags can offer error of less than 5 degrees.

Index Terms

Backscatter Radio, Direction of Arrival Estimation, Antenna Arrays.

I. Introduction

Backscatter radio is a paradigm for achieving communication in an ultra-low-power, ultra-low-complexity manner. Backscatter radio techniques exploit the reflection that an electromagnetic wave undergoes when it impinges an unmatched-to-a-load antenna [2]. The last can be exploited

The research work was supported by the Hellenic Foundation for Research and Innovation (H.F.R.I.) under the "First Call for H.F.R.I. Research Projects to support Faculty members and Researchers and the Procurement of High-cost research equipment" (Project Number: 2846). Part of this work was presented in [1]. Authors are with School of ECE, Technical Univ. of Crete, Kounoupidiana Campus, Chania, Crete, Greece 73100. tel. +30-28210-37377, email: gevougioukas@isc.tuc.gr, aggelos@telecom.tuc.gr

so as to achieve ultra-low-complexity signal conditioning tasks in the passband, just by alternating the termination of an antenna. The ultra-low-complexity & ultra-low-power nature of backscatter radio allows for ultra-low-cost devices.

A prominent application example of backscatter radio principles is commercial radio frequency identification (RFID) and relevant tags [3]. A reader provides an "illuminating" carrier signal, which, due to the backscattering operation of the RFID, will be reflected while carrying RFID's information "on top" of it. In addition to acting as "illumination", said carrier signal provides power to the tags which is harnessed using RF energy harvesting. RFID systems represent a case of *monostatic* backscatter radio deployments, where the illuminator and the receiver of the backscattered signals are co-located. Cases of *bistatic* (where the illuminator is dislocated from the receiver) backscatter radio for RFID interrogation also exist and have been examined by both industry and academia [4]–[7].

Due to its ultra-low-power & complexity character, backscatter radio has been recently exploited as a building block for IoT devices and wireless sensor networks [8], [9]. Examples of bistatic backscatter radio-based communication links and sensor network (operating at either digital or analog communication regime) deployments can be found in [10]–[12] (analog backscatter communication), [13]–[19] (digital backscatter communication). Cases of utilizing signals pre-existing in the environment for illumination (signals from FM or TV stations), namely cases of *ambient* backscatter, have been examined in [20]–[24] and references therein.

Besides achieving ultra-low-power communication, backscatter radio techniques have been recently exploited for purposes of manipulating the propagation environment [25]–[28]. A (usually) large number of controllable, reflective/backscattering elements can be deployed in a large surface. Said elements can be controlled so as to reflect an impinged signal and "focus" it at a specific location. A transmitter-receiver link can then be benefited (in terms of SNR or rate, for example) given that the receiver is located at the aforementioned location. These devices are commonly mentioned in the literature as reconfigurable intelligent surfaces (RIS). Implementation of such systems can be found in [29]–[33] and references therein.

RISs try to solve a problem that would otherwise require either a form of an active relaying system or beamforming capabilities at the transmitter (or the receiver). If conventional beamforming was to be adopted, multiple RF front ends would be required. Multiple RF front ends increase both the transmitter's (or receiver's) complexity as well as its monetary cost. In addition, it's not only beamforming that requires the existence of a number of RF front ends. A large

number of algorithms solving a variety of problems, e.g., direction of arrival estimation (DoA) estimation, multiple-input multiple output (MIMO) communication, require access to multiple observations of a signal. Towards that direction, recent studies have demonstrated the ability of a RIS to become a MIMO "transmitter"/modulator [34] and also act as a distributed array to perform target DoA estimation using a single antenna receiver [35].

Parasitic antenna arrays have also been proposed so as to mitigate the complexity associated with conventional antenna arrays and multiple RF front ends. Examples of such parasitic arrays are the switched parasitic antennas (SPAs) and electronically steerable passive array radiators (ESPARs) [36]–[38]. In such systems, a number of parasitic antenna elements are dynamically terminated with variable loads that are placed near a single active/driven element. Sufficient coupling is assured by placing the parasitic elements in the $\lambda/2$ vicinity of the active element. Given stimulation of the driven element, parasitic arrays can produce different radiation patterns by altering the termination of their parasitic elements. The operation resembles backscatter radio with the difference lying in the level of coupling between the transmitter (driven elements) and the backscattering device/tag (parasitic elements).

In addition to beamforming [39], using such antenna systems, MIMO communication [37], [38], [40], [41], multiplexing [42] and other problems requiring statistical signal processing [43], can also be solved without multiple RF front ends. An SPA for an RFID reader was designed in [44]. The circuitry of the parasitic element was wirelessly powered by the driven element, altering the parasitic load periodically.

The problem of direction of arrival (DoA) estimation was solved in [43] using a single active element (single receiving front-end) and a number of parasitics. MIMO gains were demonstrated in [38, Chap. 5], using a virtually rotating antenna. Due to the Doppler effect, a virtually rotating antenna allows for multiple "copies" of an impinged signal to appear in the frequency domain, converting spatial diversity or multiplexing (offered by a conventional antenna array) to frequency diversity (or multiplexing). Problems that would otherwise require conventional, multi-RF front end arrays, can be solved with parasitic arrays using a single RF front end. Despite lowering the complexity associated with a number of RF front ends, parasitic arrays require modifications in either the transmitter and/or the receiver of a communication system.

Motivated by the aforementioned ideas and their limitations, this work examines whether backscatter radio techniques, conventionally applied for solving ultra-low-power wireless communication problems [9], can be applied to problems requiring multiple antennas. A method

is proposed where the spatial diversity offered by a (centralized) antenna array is traded for frequency diversity offered by a deployment of a small number of single antenna, simple, switching backscattering tags. Due to the switching operation of said low-cost tags, a transmitter's signal is "copied"/relayed in distinct bands in the frequency domain [45]. A single antenna receiver can then discriminate the signals in the frequency domain and acquire independent observations of the transmitter's signal. Thus, problems requiring multiple antennas can be solved in a low-complexity manner using a single antenna receiver and multiple low-cost backscattering tags, at the expense of frequency bandwidth.

To the best of the authors' knowledge, this is the first time that backscatter radio is used in such unconventional manner: the tags act as a distributed array that aids a single antenna receiver in the direction of solving a problem requiring multiple antennas. While, as discussed earlier, a number of problems requiring multi-antenna processing can be cast and solved using the proposed multi-tag, backscatter switching-based solution, the problem of finding the direction of arrival (DoA) of a source's/transmitter's signal will be considered. Exploiting backscatter radio-based solutions to such problem(s), can allow for lower complexity and cost, by omitting the requirement for high-cost, multi-antenna receivers.

In contrast to the parasitic array approach, the proposed method does not require any modifications on the existing infrastructure i.e., modifying a single antenna receiver (or transmitter) to facilitate and control a small number of parasitic elements (in the vicinity of a single active element). Contrary to a RIS-based approach, the deployment of a small number of backscattering tags does not require large surfaces with thousands of elements and a centralized controller to manipulate them. With the proposed method, tags pre-existing in the considered space, e.g., for purposes of wireless sensing (through a backscatter radio-based, wireless sensor network) or even future RFID tags, can offer multi-antenna "services" at a single-antenna receiver.

The contributions of the work are summarized below:

- A method is proposed - for the first time to the best of the authors' knowledge - that "converts" a small number of simple, low-cost, switching backscattering tags into a distributed antenna array. Switching tags "relay" a transmitter's signal in multiple frequency bands, offering multiple independent observations to a single antenna receiver. In that way, no conventional antenna array is required at the receiver.
- The proposed idea was experimentally demonstrated in a classic multi-antenna problem, namely DoA estimation of a single RF source, using a small number of backscattering tags.

- Contrary to related RIS literature, the proposed approach does not require a large number of reflective elements and associated controllers, but instead a small number of simple backscattering tags. In addition, compared to relevant studies, the derived signal model is detailed, including many relevant parameters, experimentally tested under real-world conditions.
- Contrary to related parasitic antenna array literature, the proposed approach assumes distributed in space, wireless backscattering tags (rather than closely-placed parasitic elements) and requires - in principle - no hardware modifications at either end of a wireless communication link.
- A small number of backscattering tags were designed and built. The proof-of-concept scenario was tested under realistic indoor conditions, offering results in terms of mean absolute error (MAE).

The benefits of the proposed backscatter tag-based idea come at the cost of requiring bandwidth (for facilitating the "copies" of a transmitter's signals) and (as will be discussed in detail in subsequent chapters) means for (coarsely) synchronizing the operation of the backscattering tags. The locations of the backscattering tags must also be known, though in a non-exact manner. As the system was experimentally evaluated, the aforementioned requirements have proven to be tractable under real-world conditions. It is expected for the proposed idea not be suited for every application, but rather to pose as an alternative to tools (RISs, ESPAR) that are considered in applications with the previously discussed, hardware constraints.

The rest of the work is organized as follows. The system model is offered in Sec. II, while the processing allowing for the backscattering tags to act as a distributed array and estimate the DoA, is described in Sec. III. In Sec. IV details regarding the implementation of the backscattering tags and the single antenna receiver are given. Results of examining the performance of the system are offered in Sec. V. Finally, work is concluded in Sec. VI.

II. System Model

A. Setup

Backscatter radio is used in the setup depicted in Fig. 1, in order to assist the estimation of the DoA of a signal originating from a RF source. The RF source emits, in the general case, modulated signals. A number of single-antenna, low-cost backscattering tags are deployed in the area between the RF source and a single-antenna receiver. The latter captures both the signal

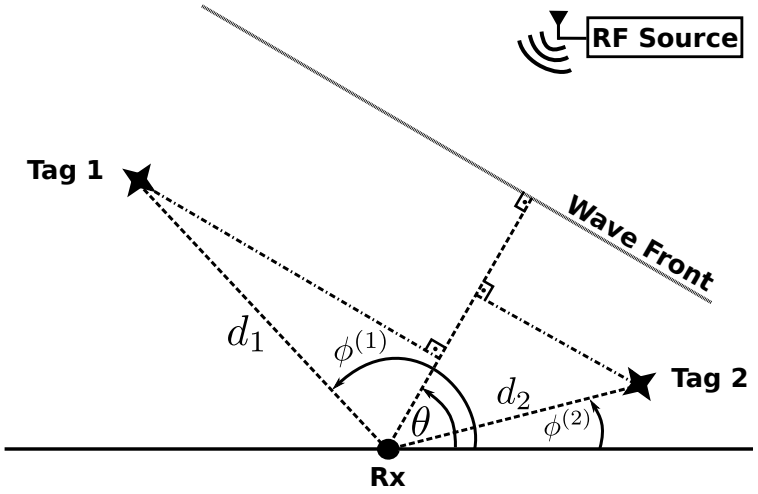

Fig. 1: Use of a number ($M = 2$) of low cost backscattering tags, along with a single antenna receiver, to estimate the angle of arrival of signal.

originating from the RF source as well as the backscattered signals, resulting from the operation of the tags. The goal for the receiver-tags system is to find the DoA of the signal stemming from the RF source.

A conventional approach to such estimation problem involves the use of an antenna array at the receiver. The outputs of such antenna array would be subsequently used by an appropriate algorithm to obtain the required estimate [46]. However, such conventional multi-antenna receiver requires a number of relatively expensive and complex RF front-ends (e.g., with designs that guarantee synchronized carrier frequency and phase among the receiving antenna elements). In the following, a method will be described so as to solve the DoA estimation problem, using a number of low-cost, wireless backscattering tags and a single-antenna receiver.

It is assumed that M backscattering tags are used. The source's signal is modelled as $\Re\left\{\mathsf{m}(t)\,\mathsf{e}^{\mathsf{j}2\pi F_{\mathrm{c}}t}\right\}$ (where F_{c} the carrier frequency and $\mathsf{m}(t)$ the complex baseband envelope) and arrives at each tag m after time-of-flight τ_{m}:

$$\tau_{\mathrm{m}} = \tau_{\mathrm{R}} - \Delta\tau_{\mathrm{m}},\ \Delta\tau_{\mathrm{m}} = \frac{d_{\mathrm{m}}\mathsf{cos}\big(\phi^{(\mathrm{m})} - \theta\big)}{c}, \tag{1}$$

where $\tau_{\mathrm{R}} = d_{\mathrm{R}}/c$ is the source-to-receiver propagation delay (Fig. 1), d_{R} is the source-to-receiver distance, c is the speed of light, tag-to-receiver distance is denoted by d_{m} and $\phi^{(\mathrm{m})}$ is the associated angle. The angle of arrival of the wavefront (signal of the RF source as it propagates in space) w.r.t. the receiver is denoted by θ (Fig. 1).

The impinged signal at tag m can be then expressed as follows [47]:

$$\begin{aligned}\Re\left\{\mathsf{c}_{\mathrm{m}}(t)\right\} &= \Re\left\{a_{\mathrm{m}}\mathsf{m}(t-\tau_{\mathrm{m}})\,\mathsf{e}^{\mathsf{j}2\pi F_{\mathrm{c}}(t-\tau_{\mathrm{m}})}\right\}\\ &= \Re\left\{a_{\mathrm{m}}\mathsf{m}(t-\tau_{\mathrm{m}})\,\mathsf{e}^{\mathsf{j}2\pi F_{\mathrm{c}}t}\mathsf{e}^{-\mathsf{j}\phi_{\mathrm{CR}}}\mathsf{e}^{\mathsf{j}2\pi\frac{d_{\mathrm{m}}\cos\left(\phi^{(\mathrm{m})}-\theta\right)}{\lambda}}\right\},\end{aligned} \tag{2}$$

where a_{m} is the amplitude attenuation of the transmitter-to-m^{th} tag link and $\phi_{\mathrm{CR}} = 2\pi F_{\mathrm{c}}\tau_{\mathrm{R}}$. It is further assumed that the signal emitted by the RF source is narrowband; in that way, $\mathsf{m}(t) \approx \mathsf{m}(t-\tau_{\mathrm{m}})\,,\ \forall\ \mathrm{m} \in \{1,\dots M\}$. Then, Eq. (2) can be simplified as follows:

$$\Re\left\{\mathsf{c}_{\mathrm{m}}(t)\right\} \approx \Re\left\{a_{\mathrm{m}}\mathsf{m}(t)\,\mathsf{e}^{\mathsf{j}2\pi F_{\mathrm{c}}t}\mathsf{e}^{-\mathsf{j}\phi_{\mathrm{CR}}}\mathsf{e}^{\mathsf{j}2\pi\frac{d_{\mathrm{m}}\cos\left(\phi^{(\mathrm{m})}-\theta\right)}{\lambda}}\right\}, \tag{3}$$

and thus, its complex baseband equivalent is given by:

$$\tilde{\mathsf{c}}_{\mathrm{m}}(t) \approx a_{\mathrm{m}}\mathsf{m}(t)\ \mathsf{e}^{-\mathsf{j}\phi_{\mathrm{CR}}}\mathsf{e}^{\mathsf{j}2\pi\frac{d_{\mathrm{m}}\cos\left(\phi^{(\mathrm{m})}-\theta\right)}{\lambda}} = a_{\mathrm{m}}\,\mathsf{m}(t)\ \mathsf{e}^{-\mathsf{j}\phi_{\mathrm{CR}}}\,\mathrm{h}_{\mathrm{m}}(\theta)\,, \tag{4}$$

where $\mathrm{h}_{\mathrm{m}}(\theta) \triangleq \mathsf{e}^{\mathsf{j}2\pi\frac{d_{\mathrm{m}}\cos\left(\phi^{(\mathrm{m})}-\theta\right)}{\lambda}}$.

It is noted that, while subsequent derivation steps assume the presence of a single line-of-sight (LOS) path, the signal model was simulated under the presence of statistical multipath components (block fading for N_{s} processing slots). Said statistical components were superimposed to the LOS path, for all the involved links during simulations.

B. Tags Switching Between Loads

A backscattering tag reflects the signal that impinges on its antenna by alternating the load that terminates the latter [8]. More specifically, assuming that signal $\Re\left\{\mathsf{c}_{\mathrm{m}}(t)\right\}$ illuminates the antenna of tag m, then the tag will backscatter a signal which can be modelled as follows [9]:

$$\Re\left\{\tilde{\mathsf{c}}_{\mathrm{m}}(t)\,\mathrm{s}_{\mathrm{m}}\left(A_{\mathrm{s}}^{(\mathrm{m})} - \Gamma_{\mathrm{m}}(t)\right)\right\}, \tag{5}$$

where $\mathrm{s}_{\mathrm{m}} \in (0,1)$ is a variable quantifying the ability of the tag to scatter the impinged power, commonly referred to as *scattering efficiency*; $A_{\mathrm{s}}^{(\mathrm{m})}$ is the *structural mode* term, a load-independent parameter defined by the tag's antenna physical characteristics [48]; $\Gamma_{\mathrm{m}}(t)$ is the reflection coefficient of the antenna-load $Z_{\mathrm{m}}(t)$ system at time instant t:

$$\Gamma_{\mathrm{m}}(t) = \frac{(Z_{\mathrm{m}}(t) - Z_{\mathrm{a}}^{*})}{(Z_{\mathrm{m}}(t) + Z_{\mathrm{a}})}, \tag{6}$$

where Z_{a} is the characteristic impedance of the tag's antenna.

Using an RF switch, each tag alternates the termination of its antenna between two loads (resulting in $\Gamma_{\mathrm{m}}(t) \in \left\{\Gamma_0^{(\mathrm{m})}, \Gamma_1^{(\mathrm{m})}\right\}$) at a rate $F_{\mathrm{sw}}^{(\mathrm{m})} = 1/T_{\mathrm{sw}}^{(\mathrm{m})}$ Hz. The process can be mathematically modelled as follows:

$$\mathsf{x}_{\mathrm{tag}}^{(\mathrm{m})}(t) = A_{\mathrm{s}}^{(\mathrm{m})} - \Gamma_{\mathrm{m}}(t) = \left(A_{\mathrm{s}}^{(\mathrm{m})} - \frac{\Gamma_0^{(\mathrm{m})} + \Gamma_1^{(\mathrm{m})}}{2}\right) + \frac{\Gamma_0^{(\mathrm{m})} - \Gamma_1^{(\mathrm{m})}}{2} b^{(\mathrm{m})}(t)\,, \tag{7}$$

where $b^{(\mathrm{m})}(t) \in \{-1, 1\}$. Using Fourier series analysis, squarewave $b^{(\mathrm{m})}(t)$ can be then expressed as follows [5], [9]:

$$b^{(\mathrm{m})}(t) = \frac{4}{\pi} \sum_{k=0}^{+\infty} \frac{1}{2k+1} \mathsf{cos}\big(2\pi(2k+1)F_{\mathrm{sw}}^{(\mathrm{m})} t + \varphi_{\mathrm{m}}\big)\,. \tag{8}$$

Due to driving the RF switch using a squarewave attaining 50% duty cycle (thus suppressing the even-numbered harmonics), the limited bandwidth at the receiver (higher order harmonics are filtered) and the fact that only the fundamental component from the switching is exploited during processing, each tag's switching signal can be modeled as follows:

$$\mathsf{x}_{\mathrm{tag}}^{(\mathrm{m})}(t) \approx m_{\mathrm{dc}}^{(\mathrm{m})}\, \mathsf{e}^{\mathsf{j}\theta_{\mathrm{dc}}^{(\mathrm{m})}} + m_{\mathrm{tag}}^{(\mathrm{m})}\, \mathsf{e}^{\mathsf{j}\theta_{\mathrm{tag}}^{(\mathrm{m})}}\, \mathsf{cos}\big(2\pi F_{\mathrm{sw}}^{(\mathrm{m})}\, t + \varphi_{\mathrm{m}}\big)\,. \tag{9}$$

The intuitive explanation for the phase φ_{m} in the above equation follows: tag m may begin switching between its loads at an arbitrary time. With respect to a reference, "zero"-phase waveform (which is defined as a square wave beginning at a rising edge), that time can be modelled through the random phase offset φ_{m}; $m_{\mathrm{dc}}^{(\mathrm{m})}\, \mathsf{e}^{\mathsf{j}\theta_{\mathrm{dc}}^{(\mathrm{m})}}$, $m_{\mathrm{tag}}^{(\mathrm{m})}\, \mathsf{e}^{\mathsf{j}\theta_{\mathrm{tag}}^{(\mathrm{m})}}$ are tag-related parameters defined (Eq. (7)) as follows:

$$m_{\mathrm{dc}}^{(\mathrm{m})}\, \mathsf{e}^{\mathsf{j}\theta_{\mathrm{dc}}^{(\mathrm{m})}} = A_{\mathrm{s}}^{(\mathrm{m})} - \left(\Gamma_0^{(\mathrm{m})} + \Gamma_1^{(\mathrm{m})}\right)/2, \tag{10}$$

$$m_{\mathrm{tag}}^{(\mathrm{m})} \mathsf{e}^{\mathsf{j}\theta_{\mathrm{tag}}^{(\mathrm{m})}} = 2\left(\Gamma_0^{(\mathrm{m})} - \Gamma_1^{(\mathrm{m})}\right)/\pi. \tag{11}$$

Assuming that the tags share the same characteristics, index m can be omitted from the aforementioned constant parameters.

III. Processing

A. Signal At The Receiver

The complex baseband signal at the single-antenna receiver, assuming homodyne reception, can be mathematically expressed as follows:

$$\mathrm{y}(t) = a_{\mathrm{CR}} \mathsf{e}^{-\mathsf{j}\phi_{\mathrm{CR}}} \mathsf{m}(t)\, \mathsf{e}^{-\mathsf{j}2\pi\Delta F t} + \sum_{\mathrm{m}=1}^{M} \mathrm{y}_{\mathrm{m}}(t) + n(t)\,, \tag{12}$$

where $a_{\rm CR}$ is the amplitude attenuation introduced by the source-to-receiver link.

Parameter ΔF models the offset between the transmitter's carrier frequency $F_{\rm c}$ and the frequency of the local oscillator at the receiver. Said offset leads to imperfect homodyne downconversion to baseband which in turn results a carrier frequency offset (CFO) term $\mathsf{e}^{-\mathsf{j}2\pi\Delta F t}$ appearing in the model. Similarly, phase offset (CPO) can be included in variable $\mathsf{e}^{-\mathsf{j}\phi_{\rm CR}}$. $n(t)$ denotes additive white Gaussian noise. Signal $\mathrm{y}_{\rm m}(t)$ models the contribution of the $\mathrm{m}^{\rm th}$ tag, expressed as follows:

$$\begin{aligned}\mathrm{y}_{\rm m}(t) &= \tilde{\mathsf{c}}_{\rm m}(t)\,\mathsf{x}_{\rm tag}^{(\rm m)}\Big(t-\tau_{\rm TR}^{(\rm m)}\Big)\,\mathrm{s}_{\rm m}\mathrm{h}_{\rm TR}^{(\rm m)}\mathsf{e}^{-\mathsf{j}2\pi\Delta F t}\\ &\overset{\text{Eq. (4)}}{\approx} \mathrm{h}_{\rm m}(\theta)\,a_{\rm m}\mathsf{m}(t)\,\mathsf{e}^{-\mathsf{j}\phi_{\rm CR}}\mathsf{x}_{\rm tag}^{(\rm m)}\Big(t-\tau_{\rm TR}^{(\rm m)}\Big)\,\mathrm{s}_{\rm m}\mathrm{h}_{\rm TR}^{(\rm m)}\mathsf{e}^{-\mathsf{j}2\pi\Delta F t}\\ &= \mathrm{h}_{\rm m}(\theta)\,a_{\rm m}\mathsf{m}(t)\,\mathsf{e}^{-\mathsf{j}\phi_{\rm CR}}\left[m_{\rm dc}\,\mathsf{e}^{\mathsf{j}\theta_{\rm dc}}+m_{\rm tag}\,\mathsf{e}^{\mathsf{j}\theta_{\rm tag}}\cos\big(2\pi F_{\rm sw}^{(\rm m)}t+\Phi_{\rm m}\big)\right]\mathrm{s}_{\rm m}\mathrm{h}_{\rm TR}^{(\rm m)}\mathsf{e}^{-\mathsf{j}2\pi\Delta F t},\end{aligned}\quad (13)$$

where $\mathrm{h}_{\rm m}(\theta)=\mathsf{e}^{\mathsf{j}2\pi\frac{d_{\rm m}\cos\left(\phi^{(\rm m)}-\theta\right)}{\lambda}}$, $\tau_{\rm TR}^{(\rm m)}=d_{\rm m}/c$ and $\mathrm{h}_{\rm TR}^{(\rm m)}=a_{\rm TR}^{(\rm m)}\mathsf{e}^{-\mathsf{j}\phi_{\rm TR}^{(\rm m)}}$ is the $\mathrm{m}^{\rm th}$ tag-to-receiver channel; $\mathrm{s}_{\rm m}$ models the scattering efficiency of the $\mathrm{m}^{\rm th}$ tag. Assuming a single line-of-sight (LOS) path, $\phi_{\rm TR}^{(\rm m)}=2\pi F_{\rm c}\tau_{\rm TR}^{(\rm m)}$. Compound phase $\Phi_{\rm m}$ is defined as $\Phi_{\rm m}\overset{\triangle}{=}\varphi_{\rm m}-2\pi F_{\rm sw}^{(\rm m)}\tau_{\rm TR}^{(\rm m)}$, where $\varphi_{\rm m}$ has been already defined at Eq. (9).

Based on Eqs. (12), (13), the signal at the receiver after sampling every $T_{\rm s}=1/F_{\rm s}$ seconds (such that $\mathrm{y}[k]=\mathrm{y}(kT_{\rm s})$) and perfect CFO correction is given by:

$$\begin{aligned}\mathrm{y}[k] &= \mathrm{h}_{\rm d}\mathsf{m}[k]+\sum_{\rm m=1}^{M}\mathrm{h}_{\rm m}(\theta)\,\mathrm{h}_{\rm TR}^{(\rm m)}\mathrm{s}_{\rm m}a_{\rm m}\mathsf{m}[k]\,m_{\rm tag}\mathsf{e}^{-\mathsf{j}\phi_{\rm CR}}\,\mathsf{e}^{\mathsf{j}\theta_{\rm tag}}\cos\big(2\pi F_{\rm sw}^{(\rm m)}\,kT_{\rm s}+\Phi_{\rm m}\big)+n(kT_{\rm s})\\ &= \mathrm{h}_{\rm d}\mathsf{m}[k]+\frac{1}{2}\sum_{\rm m=1}^{M}\mathrm{h}_{\rm m}(\theta)\,\mathrm{h}_{\rm TR}^{(\rm m)}\mathrm{s}_{\rm m}a_{\rm m}\mathsf{m}[k]\,m_{\rm tag}\mathsf{e}^{-\mathsf{j}\phi_{\rm CR}}\,\mathsf{e}^{\mathsf{j}\theta_{\rm tag}}\,\mathsf{e}^{\mathsf{j}\left(2\pi F_{\rm sw}^{(\rm m)}\,kT_{\rm s}+\Phi_{\rm m}\right)}\\ &\quad+\frac{1}{2}\sum_{\rm m=1}^{M}\mathrm{h}_{\rm m}(\theta)\,\mathrm{h}_{\rm TR}^{(\rm m)}\mathrm{s}_{\rm m}a_{\rm m}\mathsf{m}[k]\,m_{\rm tag}\mathsf{e}^{-\mathsf{j}\phi_{\rm CR}}\,\mathsf{e}^{\mathsf{j}\theta_{\rm tag}}\,\mathsf{e}^{-\mathsf{j}\left(2\pi F_{\rm sw}^{(\rm m)}\,kT_{\rm s}+\Phi_{\rm m}\right)}+n(kT_{\rm s})\,,\end{aligned}\quad (14)$$

where $\mathrm{h}_{\rm d}=a_{\rm CR}\mathsf{e}^{-\mathsf{j}\phi_{\rm CR}}+m_{\rm dc}\mathsf{e}^{\mathsf{j}\theta_{\rm dc}}\sum_{\rm m=1}^{M}\mathrm{h}_{\rm m}(\theta)\,\mathrm{h}_{\rm TR}^{(\rm m)}\mathrm{s}_{\rm m}a_{\rm m}\mathsf{e}^{-\mathsf{j}\phi_{\rm CR}}$ models the compound channel of the "direct link".

B. Signal Discrimination

Eq. (14) demonstrates the feasibility of acquiring independent observations of $\mathsf{m}[k]$, using a number (M) of simple backscattering tags and a single antenna receiver. The observations can be discriminated in the frequency domain, due to the mixing resulting from the tags' switching operation; that is manifested through the cosine terms in Eq. (14).

The discrimination can be performed using techniques commonly found in the backscatter communication literature [5], [14], [18]. Specifically, a bank of $2M$ correlators can be used to provide the necessary (for DoA estimation) output statistics. Two correlators are used per tag so as to exploit both branches of the backscattered signal (the two exponential terms in Eq. (14)) [49]. The m^{th} set $(r_{\mathrm{m}}^{+}, r_{\mathrm{m}}^{-})$ is defined as follows:

$$r_{\mathrm{m}}^{\pm} = \sum_{k=0}^{L-1} \mathrm{y}[k] \left(\mathsf{e}^{\pm \mathsf{j} 2\pi F_{\mathrm{sw}}^{(\mathrm{m})} k T_{\mathrm{s}}} \right)^{*}. \tag{15}$$

Due to the aggregate of channel terms appearing in $\mathrm{h_d}$ (which, being a DC term, does not allow discrimination of the tags' contributions), the direct link term must be removed from the signal. The removal can be achieved by the correlation process if $F_{\mathrm{sw}}^{(\mathrm{m})} \gg \mathrm{BW}(\mathsf{m}(t))$ (Appendix A) [49]. It is further assumed that $|F_{\mathrm{sw}}^{(i)} - F_{\mathrm{sw}}^{(j)}| \gg \mathrm{BW}(\mathsf{m}(t)),\ i \neq j,\ i,j \in \{1,\ldots,M\}$. It must be noted that the bandwidth requirements can be relaxed if additional filtering is applied at the receiver (prior to the correlation structure), allowing for the application of the method in signals of wider bandwidth.

Parameter T_{sl} denotes the integration time window/slot duration. It is also assumed that $F_{\mathrm{sw}}^{(\mathrm{m})} \gg \frac{1}{T_{\mathrm{sl}}}$. $L \triangleq \frac{T_{\mathrm{sl}}}{T_{\mathrm{s}}}$ is the number of samples per slot. Processing is performed over a period of N_{s} slots, i.e., a DoA estimate is acquired every $N_{\mathrm{s}} T_{\mathrm{sl}}$ seconds. As already stated, block fading applies during this period of time.

Under the aforementioned assumptions, the outputs of the $\nu^{\mathrm{th}} \in \{1 \ldots M\}$ set for the q^{th} integration slot can be expressed as follows:

$$\begin{aligned} r_{\nu,q}^{\pm} = & \frac{1}{2} \sum_{k=qL}^{qL+L-1} \mathsf{m}[k] \sum_{\mathrm{m}=1}^{M} \mathrm{h_m}(\theta)\, \mathsf{e}^{-\mathsf{j}\phi_{\mathrm{TR}}^{(\mathrm{m})}} \gamma_{\mathrm{m}} \mathsf{e}^{\mathsf{j}\Phi_{\mathrm{m}}}\, \mathsf{e}^{\mathsf{j}\left(2\pi F_{\mathrm{sw}}^{(\mathrm{m})} k T_{\mathrm{s}}\right)}\, \mathsf{e}^{\mp \mathsf{j}\left(2\pi F_{\mathrm{sw}}^{(\nu)} k T_{\mathrm{s}}\right)} \\ & + \frac{1}{2} \sum_{k=qL}^{qL+L-1} \mathsf{m}[k] \sum_{\mathrm{m}=1}^{M} \mathrm{h_m}(\theta)\, \mathsf{e}^{-\mathsf{j}\phi_{\mathrm{TR}}^{(\mathrm{m})}} \gamma_{\mathrm{m}} \mathsf{e}^{-\mathsf{j}\Phi_{\mathrm{m}}}\, \mathsf{e}^{-\mathsf{j}\left(2\pi F_{\mathrm{sw}}^{(\mathrm{m})} k T_{\mathrm{s}}\right)}\, \mathsf{e}^{\mp \mathsf{j}\left(2\pi F_{\mathrm{sw}}^{(\nu)} k T_{\mathrm{s}}\right)} \\ & + \sum_{k=qL}^{qL+L-1} n[k]\, \mathsf{e}^{\mp \mathsf{j}\left(2\pi F_{\mathrm{sw}}^{(\nu)} k T_{\mathrm{s}}\right)}, \end{aligned} \tag{16}$$

where $\gamma_{\mathrm{m}} = a_{\mathrm{TR}}^{(\mathrm{m})} \mathrm{s_m} a_{\mathrm{m}} m_{\mathrm{tag}} \mathsf{e}^{-\mathsf{j}\phi_{\mathrm{CR}}} \mathsf{e}^{\mathsf{j}\theta_{\mathrm{tag}}}$.

Theorem 1. *Utilizing results from Appendix A, the output from the correlator set corresponding to the* $\mathrm{m}^{th} \in \{1 \ldots M\}$ *tag during the the* q^{th} *integration slot, is given in the following form:*

$$r_{\mathrm{m,q}}^{\pm} = \frac{1}{2} \mathrm{h_m}(\theta)\, \mathsf{e}^{-\mathsf{j}\phi_{\mathrm{TR}}^{(\mathrm{m})}} \gamma_{\mathrm{m}} \mathsf{e}^{\pm \mathsf{j}\Phi_{\mathrm{m}}}\, \mu_{\mathrm{c}}^{(\mathrm{q})} + n_{\mathrm{m,q}}^{\pm}, \tag{17}$$

where $n_{\mathrm{m,q}}^{\pm} = \sum_{k=qL}^{qL+L-1} n[k]\, \mathsf{e}^{\mp \mathsf{j}\left(2\pi F_{\mathrm{sw}}^{(\mathrm{m})} kT_{\mathrm{s}}\right)} \sim \mathcal{CN}(0, \sigma_n^2)\,,\ \mathrm{m} \in \{1, \ldots, M\}$. Parameter $\mu_{\mathrm{c}}^{(\mathrm{q})} = \sum_{k=\mathrm{q}\cdot L}^{\mathrm{q}L+L-1} \mathsf{m}[k]$ is the sum of the source's samples during the qth integration window. Index q is omitted from the rest of the parameters by considering them invariable for the duration of N_{s} slots.

In the context of multi-tag operation, Φ_{m} models the synchronization error between the tags. As it will be shown in Sec. V, coarse synchronization between tags is required for acceptable performance; the tags must be triggered in sync to begin switching at "the same" time. A simple solution to the synchronization problem is to equip each tag with a low-cost energy detector (e.g., a diode envelope detector). The detector at each tag can trigger switching, when a transmission event occurs from the source transmitter. Impact of time synchronization error will be further quantified in Sec. V.

It is further assumed that knowledge for the locations of the tags is available, so that the associated distances can be measured up to a precision of 0.01 meters. In that way, the term $\mathsf{e}^{-\mathsf{j}\phi_{\mathrm{TR}}^{(\mathrm{m})}}$ can be (ideally) cancelled by multiplying Eq. (17) with term $\mathsf{e}^{\mathsf{j}2\pi F_{\mathrm{c}}\hat{d}_{\mathrm{m}}/c}$, where $\hat{d}_{\mathrm{m}}$ is the (measured) distance of tag m-to-receiver.

C. Emulating a Multi-Antenna Array

Assuming perfect cancellation of the tag-to-receiver channel phase $\phi_{\mathrm{TR}}^{(\mathrm{m})}$, the following statistic is derived for integration window/slot q and tag/virtual antenna element m:

$$r_{\mathrm{m,q}} = r_{\mathrm{m,q}}^{+} + r_{\mathrm{m,q}}^{-} = \mathrm{h}_{\mathrm{m}}(\theta)\, \gamma_{\mathrm{m}} \mathsf{cos}(\Phi_{\mathrm{m}})\, \mu_{\mathrm{c}}^{(\mathrm{q})} + n_{\mathrm{m,q}}, \tag{18}$$

where $n_{\mathrm{m,q}} = n_{\mathrm{m,q}}^{+} + n_{\mathrm{m,q}}^{-}$. As will be subsequently explained in Sec. V, using a single correlator instead of their sum is possible, but in such case the method becomes highly prone to synchronization (among tags) errors.

It is reminded that $\mathrm{h}_{\mathrm{m}}(\theta)$ introduces the source's DoA θ to the model (see below Eq. (4)) and Φ_{m} expresses the asynchronicity among the tags (see Eqs. (9), (13)). $\mu_{\mathrm{c}}^{(\mathrm{q})}$ models source's information signal after processing (see below Eq. (17)) which, in the general case, varies between successive integration slots. The remaining parameters are modeled through γ_{m}.

Lemma 1. *Considering γ_{m} and Φ_{m} in Eq.* (18) *block-constant for N_{s} integration slots, the*

statistics from the correlators' outputs for the q*th slot can be arranged in a vector as:*

$$\mathbf{r}_{\mathrm{q}} = \begin{bmatrix} r_1 \\ r_2 \\ \vdots \\ r_M \end{bmatrix}_{\mathrm{q}} = \mathbf{h}_{\mathrm{p}}(\theta)\, \mu_{\mathrm{c}}^{(\mathrm{q})} + \mathbf{n}_{\mathrm{q}}, \tag{19}$$

where $\mathbf{h}_{\mathrm{p}}(\theta) \triangleq (\mathbf{h}(\theta) \odot \mathbf{g})$, $\mathbf{h}(\theta) \triangleq [\mathrm{h}_1(\theta), \ldots, \mathrm{h}_M(\theta)]^{\mathrm{T}}$, $\mathbf{g} \triangleq [\gamma_1 \mathsf{cos}(\Phi_1), \ldots, \gamma_M \mathsf{cos}(\Phi_M)]^{\mathrm{T}}$, $\mathrm{q} \in \{0, \ldots, N_{\mathrm{s}} - 1\}$, $\mathbf{n}_{\mathrm{q}} \sim \mathcal{CN}(\mathbf{0}, 2\sigma_n^2 \mathbf{I}_M)$ and $\odot$ denotes the element-wise product.

The above lemma shows that exploiting a number of simple, switching, backscattering tags along with the techniques conventionally used in backscatter communication literature [9], [49], can lead to the emulation of a multi-antenna receiver system. In that way, specific instances of problems that require such receivers can be solved in a low-complexity and low-cost manner.

D. DoA Estimation

Based on Eq. (19), the autocorrelation matrix of the vector $\mathbf{r}_{\mathrm{q}}$, $\mathbb{E}\big[\mathbf{r}_{\mathrm{q}}\mathbf{r}_{\mathrm{q}}^{\mathrm{H}}\big]$, can be expressed as:

$$\mathbf{R} = \mathbb{E}\big[\mathbf{r}_{\mathrm{q}}\mathbf{r}_{\mathrm{q}}^{\mathrm{H}}\big] = \widetilde{\mathbf{R}} + 2\sigma_n^2 \mathbf{I}_M, \tag{20}$$

where $\mathbf{I}_M$ is the $M \times M$ identity matrix. The $(i,j)^{\text{th}}$ element of matrix $\widetilde{\mathbf{R}}$ can be evaluated as follows:

$$\begin{aligned} \widetilde{R}_{(i,j)} &= \mathrm{h}_i(\theta)\, \mathrm{h}_j^*(\theta)\, \mathbb{E}\big[\gamma_i \gamma_j^*\big]\, \mathbb{E}[\mu_{\mathrm{c}} \mu_{\mathrm{c}}^*]\, \mathbb{E}[\mathsf{cos}(\Phi_i)\, \mathsf{cos}(\Phi_j)] \\ &= \mathrm{h}_i(\theta)\, \mathrm{h}_j^*(\theta)\, \mathbb{E}\big[\gamma_i \gamma_j^*\big]\, \mathbb{E}\big[|\mu_{\mathrm{c}}|^2\big]\, \mathbb{E}[\mathsf{cos}(\Phi_i)]\, \mathbb{E}\left[\mathsf{cos}(\Phi_j)\right], \;\; i, j \in \{1, 2, \ldots M\}. \end{aligned} \tag{21}$$

Eq. (21) shows that, in order to avoid cross terms attaining relatively small values (compared to the diagonal entries), $\mathbb{E}[\mathsf{cos}(\Phi_i)]\, \mathbb{E}\left[\mathsf{cos}(\Phi_j)\right]$ should be sufficiently large, compared to $\mathbb{E}\left[\mathsf{cos}^2(\Phi_i)\right]$. This, as it will be also discussed in more detail in Sec. V-A and Sec. V-A1, is the mathematical view of the requirement for synchronisation among the tags, described in the previous subsection.

In practice, matrix $\mathbf{R}$ is not available. Thus, the processing is performed using an estimate $\widehat{\mathbf{R}}$ of $\mathbf{R}$. $\mathbf{Y} = [\mathbf{r}_1, \ldots, \mathbf{r}_{N_{\mathrm{s}}}]$ is defined and eigenvalue decomposition is applied to the estimated autocorrelation matrix $\widehat{\mathbf{R}} = \frac{1}{N_{\mathrm{s}}} \mathbf{Y}\mathbf{Y}^{\mathrm{H}}$:

$$\widehat{\mathbf{R}} = \mathbf{Q}\mathbf{\Lambda}\mathbf{Q}^{-1}. \tag{22}$$

Assuming a single RF source and $N_{\mathrm{s}} \geq M$, the eigenvector $\mathbf{q}_{\mathrm{s}} \in \mathbb{C}^{M\times 1}$ corresponding to the largest eigenvalue spans the signal subspace. The remaining $M-1$ eigenvectors are arranged in a matrix $\mathbf{Q}_n \in \mathbb{C}^{M\times M-1}$ and are utilized for the retrieval of an angle spectrum as per MUSIC algorithm [50]:

$$\mathsf{P}(\theta) = \frac{1}{||\mathbf{Q}_{\mathrm{n}}^{\mathrm{H}}\mathbf{h}(\theta)\,||^2}. \tag{23}$$

Assuming a source having a true DoA of θ_{s}, an estimate of said DoA can be obtained as:

$$\hat{\theta}_{\mathrm{s}} = \arg \max_{\theta\in[\theta_{\min},\theta_{\max})} \mathsf{P}(\theta)\,, \tag{24}$$

where $\theta_{\min}$, $\theta_{\max}$ are variables defining the search space.

IV. Proof-of-Concept Implementation

A. Tags

1) Load Switching: Each tag m must be able to alter the termination of its antenna between two loads at a rate of $F_{\mathrm{sw}}^{(\mathrm{m})}$ Hz. The switching between loads is achieved using an Analog Devices ADG919 RF switch. The antenna of the tag is directly connected to the switch; based on an external squarewave signal, the switch either shorts or opens the antenna terminals, offering two reflection coefficients Γ_0 and Γ_1, such that $\Gamma_0 = -\Gamma_1 = 1$.

2) Producing the Switching Signal: The switching signal is generated by a Silicon Laboratories 8051F320 microcontroller (MCU). To produce the switching signal, the MCU asserts the line driving the RF switch high, burns a number of cycles using an appropriate number of *no operation* (NOP) instructions and then de-asserts the line. Line de-assertion is also followed by a number of NOP instructions. The process runs iteratively to facilitate the periodicity of the produced squarewave signal.

Both the frequency ($F_{\mathrm{sw}}^{(\mathrm{m})}$) and the duty cycle of the produced squarewave signal are controlled by the number and balance[1] of NOP instructions used. The number of NOPs was trimmed to attain the required frequency ($F_{\mathrm{sw}}^{(\mathrm{m})}$) and duty cycle (which was set to 50% in order to eliminate the even-numbered harmonics) using an oscilloscope. The switching frequencies of the tags are offered in Table I. The choice of producing delays by burning MCU cycles, instead of using a timer, was made in order to avoid any unexpected operations (e.g., handling an interrupt) that would result in producing incorrect switching waveforms.

[1]The balance refers to the number of NOPs used prior to and post line de-assertion.

TABLE I: Switching frequencies utilized by the backscattering tags.

Tag #	Switching Frequency (kHz)
1	137.5
2	281
3	170
4	102.5
5	240

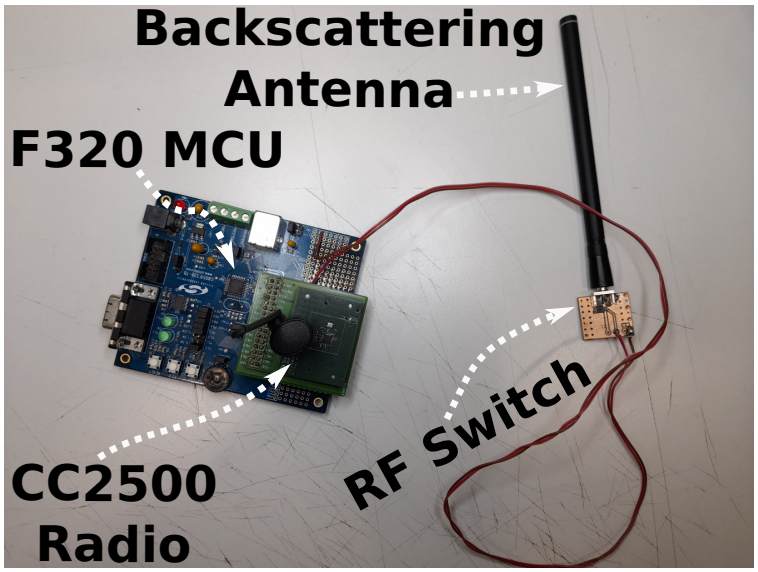

Fig. 2: Each backscattering tag is comprised of a F320 MCU for producing the necessary switching signals, a CC2500 radio for synchronized operation with the rest of the tags and an RF switch for backscattering.

3) Synchronizing the tags: As stated in Sec. III, synchronization among the tags is required. In this implementation, each tag is equipped with a Texas Instruments CC2500 embedded radio IC. The CC2500 is connected to the MCU and the MCU initiates the switching operation when a specific packet is received by the CC2500 radio. A "central" node is used, sharing the same architecture with the tags (8051F320 & CC2500, see Fig. 2). The central node transmits a packet in the 2.4 GHz band which is received by all the tags. Once the packet is received, the tags begin their switching operation. The method provided sufficient synchronization allowing for the system to offer acceptable results (i.e., to demonstrate that the idea is feasible). Oscilloscope captures for the degree of synchronization between 3 tags are offered in Fig. 3.

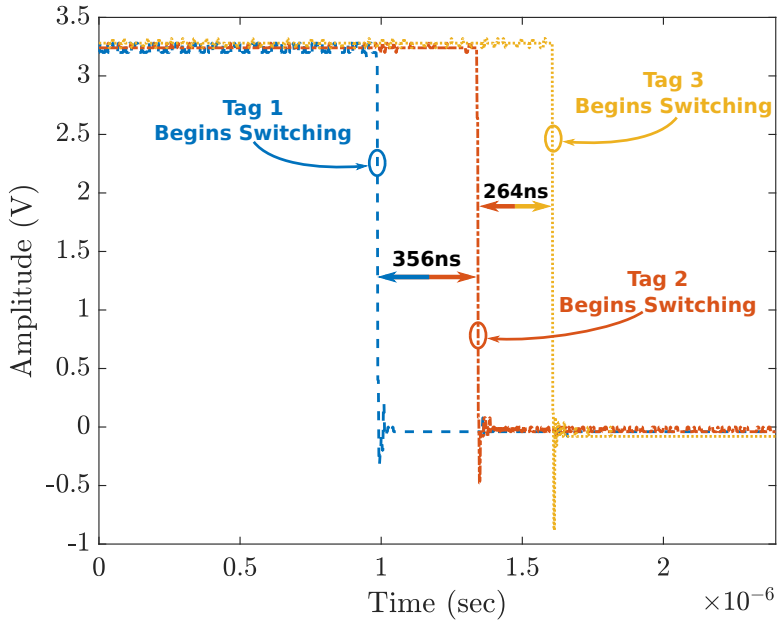

Fig. 3: Switching waveforms for 3 tags after receiving the initiation packet from the central node. The waveforms were captured using an oscilloscope. The time offsets accounted for a maximum of 10% of the tags' switching period.

It was observed that the timing offset among tags varied between "runs"/experiments. Additionally, in the majority of the experiments for ≤ 4 tags, sufficient synchronization was always achieved. In most of the cases, significant synchronization mismatch was observed when adding over 4 tags. The problem was attributed to the fact that as the number of tags increased, (relatively) higher switching frequencies were required, which, in conjunction with the requirement for synchronization with the rest of the tags, proved difficult given the hardware constraints and the limited resources of the F320 MCU.

It is noted that the use of embedded radios for synchronization (between the backscattering tags) purposes, was solely made for quickly demonstrating the feasibility of the proposed concept. Further work is required for developing low-complexity, low-cost, energy-based detectors for synchronising the tags.

B. Single-antenna Receiver & Processing

1) Receiver: An RF generator is used as the RF source. The generator was configured to produce an unmodulated carrier at $F_{\mathrm{c}} = 868$ MHz and a power output of $P_{\mathrm{tx}} = 23$ dBm. A

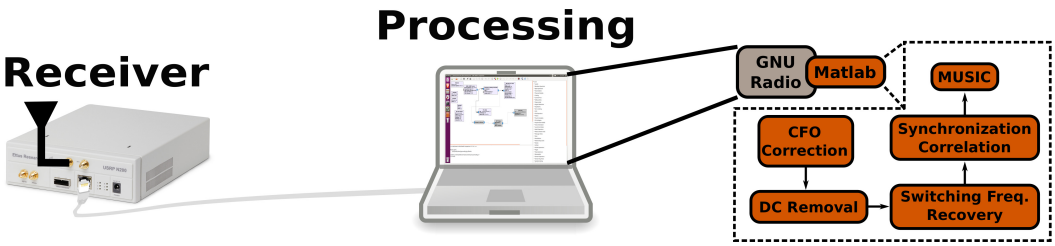

Fig. 4: Block diagram of the signal processing chain for the proof-of-concept setup.

USRP N200 SDR was used to provide the baseband samples required for further processing. The USRP was equipped with an SBX daughterboard and was tuned at 868 MHz.

2) Processing: The raw samples from USRP are saved to a file using GNURadio. The samples are then read by a Matlab script and the processing described in Sec. III is performed. The script performs the following steps in order to estimate the DoA of the RF source:

1) CFO Correction: Periodogram estimation is applied to the samples, using fast Fourier transform (FFT) and the frequency where the highest peak is observed is used for cancelling the effect of CFO.
2) DC Removal: In order to remove the DC component of the signal after CFO correction, numerical averaging is used. The obtained value is subtracted from the CFO corrected samples. The process is required for the case of a CW source; for a modulated RF source, the direct link term is removed subsequently by the correlation process (see Sec. III, [49]).
3) Recovery of Switching Frequencies: The exact switching frequencies of the tags are recovered using the same techniques utilized during CFO correction, iteratively, i.e., until the frequencies for all tags are obtained.
4) Synchronization and Correlation: The received signal is convolved with the basis functions, i.e., the complex exponentials rotating at the switching frequencies of the tags. The result of the correlation is obtained at the time instant dictated by the synchronization step.
5) MUSIC processing: The MUSIC algorithm is applied to the statistics (modelled by Eq. (18)) resulting from the correlation process.

The process is also depicted in Fig. 4. The processing is performed on "packets" of $N_{\mathrm{s}} = 30$ slots with each slot containing $L = 1000$ samples. The sampling rate at the USRP was configured at $F_{\mathrm{s}} = 1$ MSamples/sec.

V. Numerical Results

A. Simulations

The feasibility of the proposed concept was initially examined using simulations. The root mean squared error (RMSE) was considered as a performance indicator, averaged over 10^4 geometrically different tag and source deployments (receiver was set at the origin). Each deployment was randomly realized as $d_{\mathrm{m}} \sim \mathcal{U}[1, 20]$ m, $\phi^{(\mathrm{m})} \sim \mathcal{U}[0, \pi]$, $d_{\mathrm{R}} \sim \mathcal{U}[20, 30]$ m, while the source's DoA was calculated as $\theta_{\mathrm{s}} \sim \mathcal{U}[0, \pi]$ (different θ_{s} per experiment). Source-to-tags distances were calculated using the aforementioned variables.

The duration of a "packet" was set to $N_{\mathrm{s}} = 30$ slots. For the case of an unmodulated (CW) RF source, the sampling rate was set to $F_{\mathrm{s}} = 1$ MHz with $L = 10^3$, while for the case of a modulated source $F_{\mathrm{s}} = 4$ MHz with $L = 4000$. The aforementioned values result in a packet duration of $N_{\mathrm{s}} L T_{\mathrm{s}} = 30$ ms, which satisfies the block fading requirement in limited-mobility, indoor environments.

The tag related phase φ_{m} was modelled as $\varphi_{\mathrm{m}} \sim \mathcal{N}(0, \sigma_{\mathrm{sw}}^2)$, where $\sigma_{\mathrm{sw}} = \rho\, 2\pi F_{\mathrm{sw}}^{(\mathrm{m})} T_{\mathrm{sw}}^{(\mathrm{m})}$ with $\rho \in [0, 1]$. Phase φ_{m} characterizes the tag synchronization mismatch, as a percentage of each tag's switching period. That way, standard deviation σ_{sw} can define the degree of synchronization mismatch among the tags. Given that exact behaviour of each tag can not be easily predicted, a stochastic modelling of the mismatch is more appropriate, besides, (approximate) deterministic modelling can be achieved through a fixed-mean, low-variance Gaussian distribution.

For the tag-to-reader link "cancellation", $\hat{d}_{\mathrm{m}}$ was modelled as $\hat{d}_{\mathrm{m}} \sim \mathcal{N}\left(d_{\mathrm{m}}, \left(10^{-2}\right)^2\right)$. Tag RF parameters were chosen as $\Gamma_0 = \Gamma_0^{(\mathrm{m})} = -\Gamma_1^{(\mathrm{m})} = -\Gamma_1 = 1$, $A_{\mathrm{s}} = A_{\mathrm{s}}^{(\mathrm{m})} = 0.6047 + \mathrm{j}0.5042$ and $\mathrm{s}_{\mathrm{m}} \sim \mathcal{N}\left(\sqrt{0.1}, 0.05^2\right)$.

The wireless channel parameters were statistically modelled according to unit-variance, Rician fading. The LOS paths described in previous sections were used as the dominant paths. The Rice parameters for the involved links (ST, TR) were set to 10 ($\mathrm{K}_{\mathrm{ST}} = \mathrm{K}_{TR} = 10$, unless otherwise noted). Large-scale pathloss was also included in the model with a pathloss exponent of 2.2 [51]. SNR is defined according to Eq. (18), as the minimum SNR across all tags.

An instance of a MUSIC-based DoA spectrum acquired from a single packet of N_{s} slots (referred to as "Single Shot Spectrum") is offered in Fig. 5. In the same figure, an averaged over 20 packets spectrum is offered. The rest of the results (from simulations) are acquired after averaging the acquired spectrum over 20 packets.

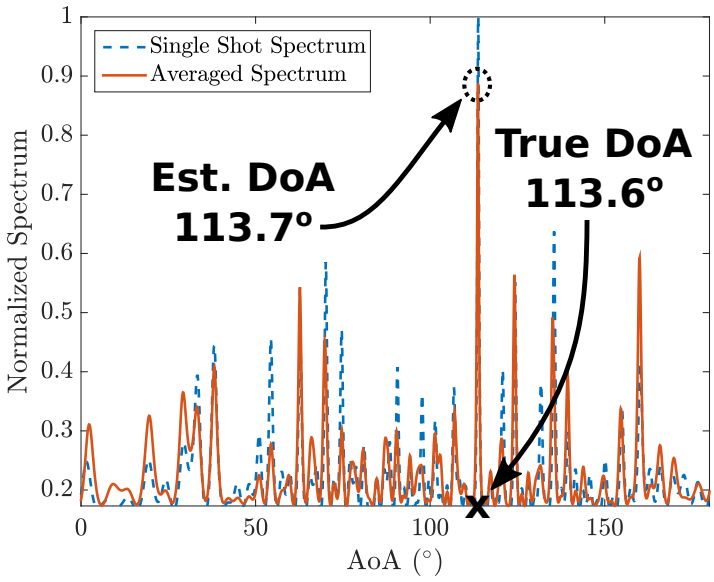

Fig. 5: Single shot and averaged (over 20 packets) MUSIC spectrum for $M = 5$ tags, $\rho = 0.1$ and SNR$= 10$dB. The abscissa denotes the DoA measured in degrees (angle of arrival/AoA).

The RMSE performance of the system, as a function of the number of tags utilized is offered in Fig. 6, for two degrees of synchronization mismatch ($\rho = 0.05$ and $\rho = 0.1$). The results are for the case of an unmodulated RF source, i.e., $\mathsf{m}[k] = A_{\mathrm{c}}\mathsf{e}^{\mathrm{j}\phi_{\mathrm{c}}}$. The results depicted in Fig. 6 show that as the number of tags increases, the performance drastically improves up to a saturation point (for > 9 tags). The performance gain (w.r.t. RMSE) associated with increasing the number of tags, comes at the cost of higher bandwidth so as to facilitate the switching subcarriers ($F_{\mathrm{sw}}^{(\mathrm{m})}$) of said tags.

In the same figure, the performance gap between utilizing the output of only r_{m}^{+} and utilizing the aggregate $r_{\mathrm{m}}^{+} + r_{\mathrm{m}}^{-}$ is shown. It can be seen that the gap is more pronounced for higher synchronization mismatch. The behaviour can be attributed to the fact that, utilizing only a single correlator leads to the presence of a strong diagonal component (due to the term $\mathsf{e}^{\pm\mathrm{j}\Phi_{\mathrm{m}}}$, see Eqs. (17),(21)) in $\widetilde{\mathbf{R}}$. The aforementioned component is constant and independent of any other variable. Thus, the combination of lower values in the cross-correlation terms (resulting from the increased synchronization mismatch) and the aforementioned constant, diagonal component limits the rank deficiency of $\widetilde{\mathbf{R}}$. The effect can be better understood by looking at Fig. 7. If a single correlator is used (e.g., r_{m}^{+}), the diagonal term $\mathbb{E}\left[\mathsf{e}^{\mathrm{j}\Phi_{\mathrm{m}}}\left(\mathsf{e}^{\mathrm{j}\Phi_{\mathrm{m}}}\right)^{*}\right] = 1$ will dominate the

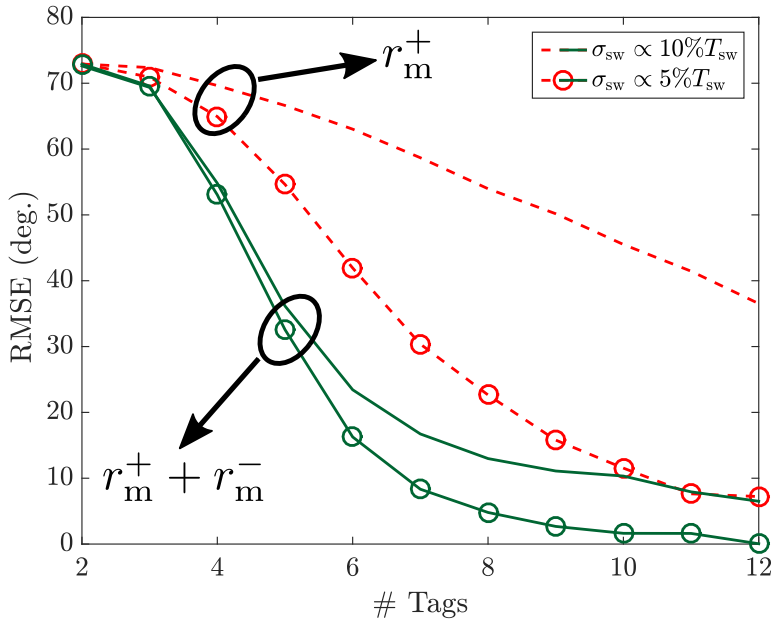

Fig. 6: RMS error (in degrees) as a function of the number of tags utilized for SNR $= 10$ dB. Cases for two different values of ρ (adjusting the synchronization mismatch among the tags) are offered, namely $\rho = 0.1$ and $\rho = 0.05$. The performance for the case of exploiting only one correlator output (r_{m}^{+}) or the sum of $r_{\mathrm{m}}^{\pm}$, is also depicted.

off-diagonal terms, as synchronization mismatch σ_{sw} increases.

The sensitivity of the system to the synchronization mismatch between the tags was examined and the results are offered by Fig. 7. The time window/"phase sector" within which the tags where synchronized, was varied by adjusting the standard deviation σ_{sw}.

1) Analytical Considerations regarding Tag Synchronisation: The impact of synchronisation mismatch to the performance of the system, manifests itself (mathematically) in the entries of the autocorrelation matrix, through terms $\mathbb{E}[\cos(\Phi_i)]\,\mathbb{E}[\cos(\Phi_j)]$ and $\mathbb{E}[\cos^2(\Phi_i)]$ (as shown in Eq. (21)).

As described in the beginning of this section, phases are statistically modelled through φ_{m}. Given a CW source, the switching frequencies of the tags are assumed in the order of 100 kHz. In conjunction with the distances involved, it can be safely assumed that $2\pi F_{\mathrm{sw}}^{(\mathrm{m})} \tau_{\mathrm{m}}^{'} \approx 0$ and $\Phi_{\mathrm{m}} \approx \varphi_{\mathrm{m}}$ (for analytical considerations only). To simplify the analytical expressions, the propagation term has been ignored.

The results in Fig. 7 show that, depending on the number of tags and the error requirements,

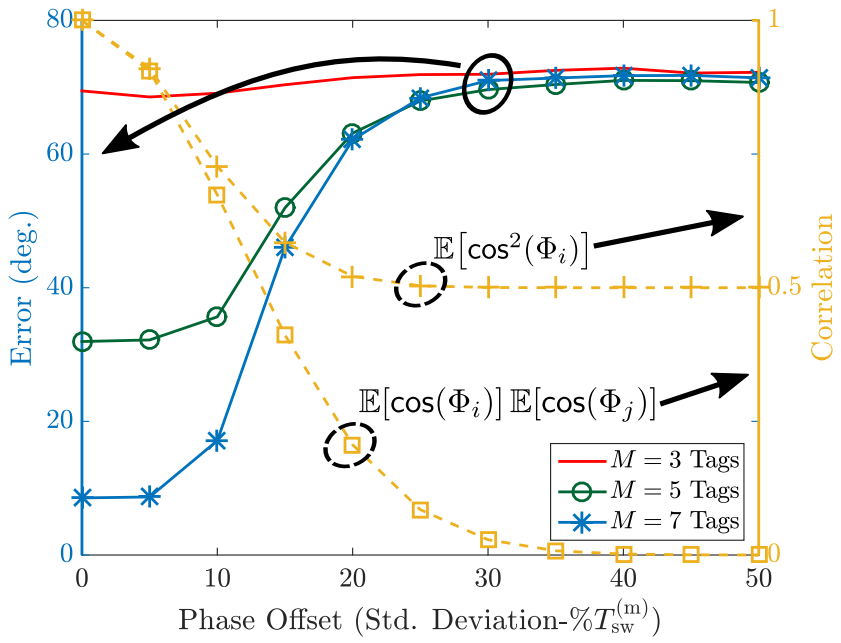

Fig. 7: RMS error (in degrees) vs the standard deviation defining the synchronization mismatch, for SNR $=$ 10 dB. Cases for $M = 3, 5, 7$ tags are given. The standard deviation $\sigma_{\rm sw}$ is varied as a percentage $\rho \in [0, 0.5]$ of $T_{\rm sw}^{(\rm m)}$. The analytical expressions for $\mathbb{E}[\cos^2(\Phi_i)]$ and $\mathbb{E}[\cos(\Phi_i)]\,\mathbb{E}[\cos(\Phi_j)]$ are also shown. It is noted that Monte-Carlo evaluation of the aforementioned expected values, produces results that match exactly the analytical calculations. Monte-Carlo results are omitted for reasons of figure clarity.

a synchronization mismatch of up to 10% can be tolerated. Small values of $\sigma_{\rm sw}$ (little to none mismatch), confine variables $\varphi_{\rm m}$ into a narrower range. Such confinement leads both the auto and cross-correlation terms (in $\widetilde{\mathbf{R}}$) to attain significant values, limiting the problems mentioned in previous paragraphs. It is noted that the performance degradation observed for a larger number of tags (error increases when going from 5 to 7 tags, for example) is due to the fact that it is harder for a large number of tags to be synchronized, when the mismatch deviation is increased (see [32]).

As stated earlier, diagonal dominance in $\widetilde{\mathbf{R}}$ is a problem. Due to the statistical modelling of $\varphi_{\rm m}$ (and by extension $\Phi_{\rm m}$), it can be analytically shown (see Appendix B) that $\mathbb{E}[\cos^2(\Phi_i)] = \frac{1}{2}\left(1 + \mathrm{e}^{-2\sigma_{\rm sw}^2}\right)$ and $\mathbb{E}[\cos(\Phi_i)]\,\mathbb{E}[\cos(\Phi_j)] = \mathrm{e}^{-\sigma_{\rm sw}^2}$ ($\Phi_{\rm m} \approx \varphi_{\rm m}$). It is clear from the aforementioned definitions that as $\sigma_{\rm sw}$ increases, $\mathbb{E}[\cos^2(\Phi_i)]$ will flatten out at $1/2$, while

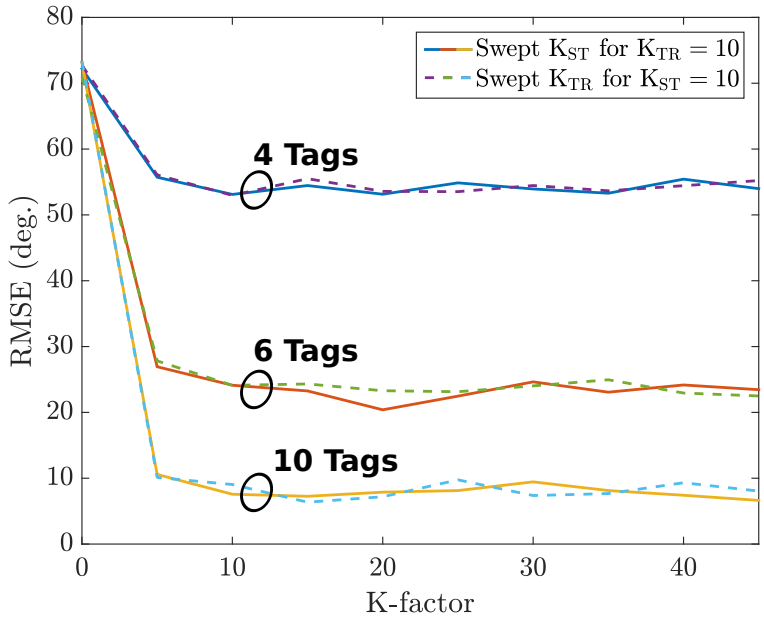

Fig. 8: RMS error (in degrees) vs the K-factor defining the power ratio of the dominant (LOS) path to the rest of the multipath components. Cases for $M = 4, 6, 10$ tags are given for SNR $= 10$ dB and $\rho = 0.1$ (synchronization mismatch of 10%).

$\mathbb{E}[\cos(\Phi_i)]\,\mathbb{E}[\cos(\Phi_j)]$ diminishes to zero (Fig. 7). Thus, the difference between the two terms (diagonal and off-diagonal) will tend to increase up to a saturation point, which explains the performance observed in Fig. 7. Results shown in Fig. 7 demonstrate that the behaviour of the aforementioned analytical expressions, predicts the performance of the system as a function of the degree of synchronization mismatch among the tags.

It is worth mentioning that the starting state of the tags (i.e., if the phase with which the squarewave "starts") is irrelevant as long as they are synchronized. The last can be mathematically expressed as a constant term appearing within each φ_{m}. In such case it can be shown that the error behaviour remains the same.

Multipath fading in the source-to-tag (ST) links, results in "ghost sources" appearing in the angle spectrum, with each "ghost source" representing a reflection undergone by the actual source signal. Fig. 8 offers the performance of the system as a function of the Rice factors $\mathrm{K}_{\mathrm{ST,TR}}$. As it is expected, increasing the power ratio between the dominant/line-of-sight path and the reflected signal paths, offers better performance. Channel states attaining a high-valued K-factor, resemble scenarios where multipath is absent. As stated earlier, fading is also assumed for the

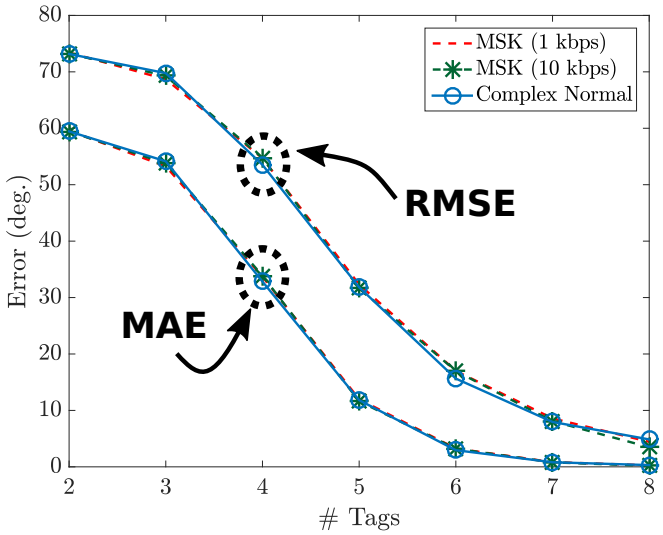

Fig. 9: RMS & MA error (in degrees) vs number of tags for SNR $= 10$ dB, $\rho = 0.05$ and modulated source signals. 2 cases of MSK modulated signals are examined. The performance of when modelling the source's baseband samples as samples drawn from a complex normal distribution is also shown.

tag-to-receiver (TR) links. The last can be viewed as noise distinctively affecting each element of the steering vector and thus, further contributing to the appearance "false" peaks in the angle spectrum.[2]

3) Modulated RF Source: The performance of the system w.r.t. RMSE and mean absolute error (MAE) for the case of a source emitting modulated signals, is offered in Fig. 9. MSK of two different rates was utilized as source modulation. The case of modelling the source's complex baseband envelope as $\mathsf{m}[k] \sim \mathcal{CN}(0, \sigma_{\mathrm{c}}^2)$ (where σ_{c}^2 the source's transmission power), was also examined. The performance of the system is similar to the performance offered in the case of an unmodulated RF source.

Fig. 10: Antenna array comprised of backscattering tags. The switching frequency of each tag is offered in Table I. Due to failure to achieve synchronization with the other tags during the experiments, tag #6 was omitted.

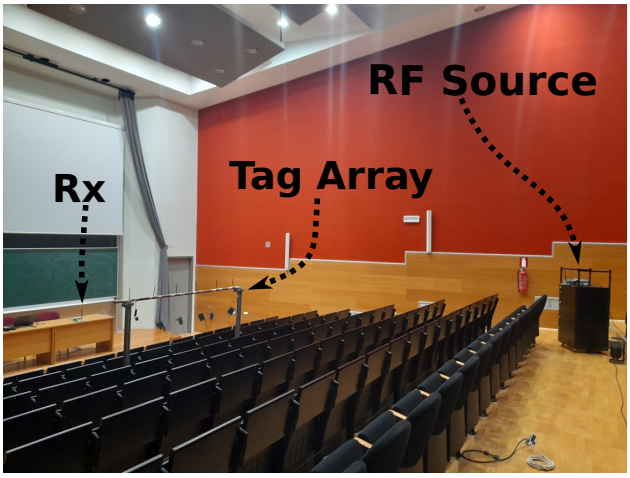

Fig. 11: Deployment of the proof-of-concept implementation in an indoors environment (amphitheatre).

B. Experiments

The proof-of-concept system presented in Sec. IV was used in order to further examine the feasibility of the system in a real deployment. The tags were deployed in a linear array-like

[2]The effect can be studied in a manner similar to how the impact of synchronization mismatch is studied: by examining the contribution of statistical fading in each element of the autocorrelation matrix.

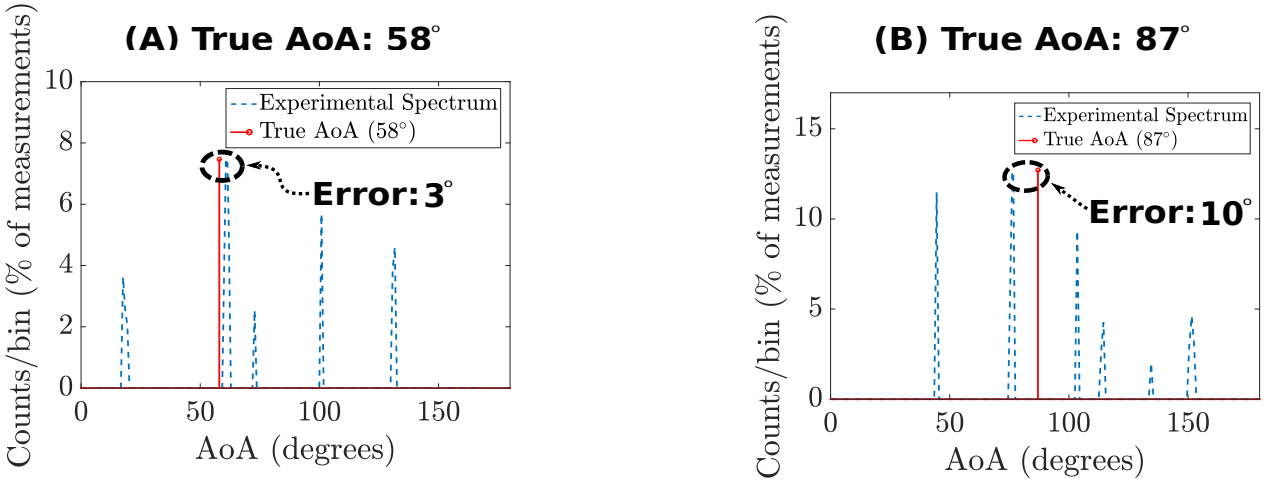

Fig. 12: Experimental results for two different cases of DoA utilizing 4 tags. The counts per bin are expressed as the percentage of total DoA acquisitions/measurements during a time period of 2 minutes. The abscissa denotes the DoA measured in degrees (angle of arrival/AoA).

arrangement in an amphitheatre (indoors, see Fig. 10), 4.1 meters away from the receiver. The exact distance and angle of each tag with respect to the receiver was calculated using geometry and a laser rangefinder. The setup is depicted in Fig. 11. Details regarding the adopted receiver and generator settings can be found in Sec. IV.

The RF source was placed in 3 different locations offering $58°$, $87°$ and $115°$ of DoA, respectively. The true DoAs of the source were measured using a digital angle-finder, whose reports served as ground-truth measurements. For each location the SDR was used to record the samples at a rate of 1 MHz for two minutes. The processing was subsequently performed offline (see Sec. IV). For each location three sets of recordings were acquired.

The processing was applied on packets of $N_{\mathrm{s}} = 30$ integration slots with each slot integrating over $L = 10^3$ samples. MUSIC was applied to each packet and an "averaged" DoA spectrum was offered every 2 packets. A DoA estimate was obtained from said average spectrum using Eq. (24).

The results are offered as a histogram of the acquired DoA estimates over a period of 2 minutes. The histogram utilizes 180 bins and it is filtered in the sense that it only shows bins whose associated counts are over 2% of the total number of DoA acquisitions. Results for when utilizing 4 tags for 2 different DoAs in a single experiment, are offered in Fig. 12.

The behaviour of the system as a function of the number of tags utilized during the experiments

is offered in Fig. 13. The results are averaged errors over all the locations and set of recordings. In the same plot the error resulting from simulation runs (with simulation parameters matching those of the experimental setup) is depicted. The expected decreasing (w.r.t. the error) trend is observed in the experimental results. The gap between the experimental and simulation results is attributed to two factors: a) imperfect knowledge of the tag's exact locations (affecting the definition of $\mathbf{h}(\theta)$) and b) the degree of synchronization mismatch may vary between each experiment and thus it is not easy to measure and model it, in an exact manner, within the simulation environment.

It is noted that while 6 tags were originally utilized (and depicted in Fig. 10), tag #6 was not used due to significant synchronization mismatch and failure to maintain a stable switching frequency. Taking into account results from both Fig. 13 and Sec. V-A, in practice, more than 6 tags are required to achieve acceptable performance (i.e., small MAE).

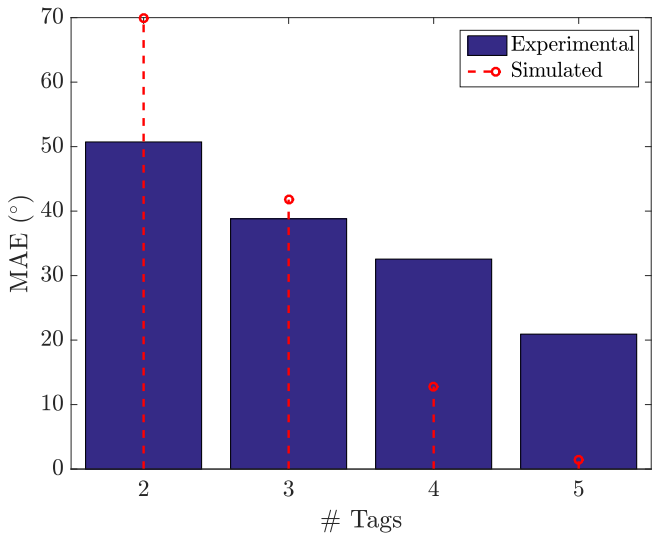

Fig. 13: MAE (in degrees) as a function of the number of tags utilized during the experiments. The MAE obtained from simulations utilizing parameters describing the experimental setup, is also offered.

VI. Conclusion

It was demonstrated for the first time (to the best of the authors' knowledge) that backscatter radio can be used in an unconventional manner, providing array functionality to a single

antenna receiver, without the cost and complexity associated with multiple RF front ends. Solving problems requiring multiple observations with the presented backscatter radio techniques, lowers cost, complexity and power consumption. While this work addressed the DoA estimation problem, future work can contribute to other problems that would traditionally be solved with conventional arrays. By exploiting backscattering switching techniques in unconventional ways, backscatter radio finds perhaps a new area for applications and research.

APPENDIX A
FILTERING OF THE DIRECT SIGNAL COMPONENT

The expression in Eq. (16) can be significantly simplified if, due to the related bandwidth assumptions, the following are taken into account [47, Chap. 3.2]:

- If $F_{\mathrm{sw}}^{(\mathrm{m})} \gg \mathrm{BW}(\mathsf{m}(t))$ then $\sum_{k=qL}^{qL+L-1} \mathsf{m}[k]\, \mathsf{e}^{\pm \mathsf{j}\left(2\pi F_{\mathrm{sw}}^{(\mathrm{m})}\, kT_{\mathrm{s}}\right)}$ attains negligible values compared to $\sum_{k=qL}^{qL+L-1} \mathsf{m}[k]$. Thus it can be assumed that:
$$\sum_{k=qL}^{qL+L-1} \mathsf{m}[k]\, \mathsf{e}^{\pm \mathsf{j}\left(2\pi F_{\mathrm{sw}}^{(\mathrm{m})}\, kT_{\mathrm{s}}\right)} \approx 0. \tag{25}$$
- Similarly, if $|F_{\mathrm{sw}}^{(\mathrm{m})} - F_{\mathrm{sw}}^{(\nu)}| \gg \mathrm{BW}(\mathsf{m}(t))$ then the following can be assumed:
$$\sum_{k=qL}^{qL+L-1} \mathsf{m}[k]\, \mathsf{e}^{\pm \mathsf{j}\left(2\pi \left(F_{\mathrm{sw}}^{(\mathrm{m})} - F_{\mathrm{sw}}^{(\nu)}\right) kT_{\mathrm{s}}\right)} \approx 0,\ \mathrm{m} \neq \nu,\ \mathrm{m}, \nu \in \{1, \ldots, M\}\,. \tag{26}$$
- For the case of a CW RF source, it suffices that $|F_{\mathrm{sw}}^{(\mathrm{m})} - F_{\mathrm{sw}}^{(\nu)}| = \frac{\mathrm{k}}{T_{\mathrm{sl}}},\ \mathrm{k} \in \mathbb{N}$.

The aforementioned definitions hold because of the following. A relatively "slow" $\mathsf{m}[k]$ modulates a "fast" exponential term. Another way of looking at the results of the assumptions is viewing the term $\sum_{k=qL}^{qL+L-1} \mathsf{m}[k]\, \mathsf{e}^{-\mathsf{j}\left(2\pi F_{\mathrm{sw}}^{(\mathrm{m})}\, kT_{\mathrm{s}}\right)}$ as an approximation to the Fourier transform of $\mathsf{m}(t)$ at frequency $F_{\mathrm{sw}}^{(\mathrm{m})}$. If the frequency content of $\mathsf{m}(t)$ is limited below $F_{\mathrm{sw}}^{(\mathrm{m})}$ (i.e. $F_{\mathrm{sw}}^{(\mathrm{m})} > \mathrm{BW}(\mathsf{m}(t))$), then, theoretically, said term would result in zero. In practice however, signals may extend well beyond their theoretical bandwidth leading to the requirement for a sufficiently greater switching frequency ($F_{\mathrm{sw}}^{(\mathrm{m})} \gg \mathrm{BW}(\mathsf{m}(t))$.

APPENDIX B
EVALUATION OF $\mathbb{E}[\mathsf{cos}^2(\varphi_{\mathrm{m}})]$ AND $\mathbb{E}[\mathsf{cos}(\varphi_{\mathrm{m}})]$

The cosine term can be rewritten form as $\mathsf{cos}^2(\varphi_{\mathrm{m}}) = \frac{1}{2}\left(1 + \mathsf{cos}(2\varphi_{\mathrm{m}})\right)$. Exploiting the complex exponential form of the cosine function, $\mathbb{E}[\mathsf{cos}^2(\varphi_{\mathrm{m}})]$ can be then expressed as:
$$\mathbb{E}\left[\mathsf{cos}^2(\varphi_{\mathrm{m}})\right] = \frac{1}{2}\left(1 + \mathbb{E}[\mathsf{cos}(2\varphi_{\mathrm{m}})]\right) = \frac{1}{2}\left(1 + \frac{1}{2}\mathbb{E}\left[\mathsf{e}^{\mathsf{j}2\varphi_{\mathrm{m}}} + \mathsf{e}^{-\mathsf{j}2\varphi_{\mathrm{m}}}\right]\right). \tag{27}$$

The characteristic function $M_x(\mathsf{j}) = \mathbb{E}\big[\mathsf{e}^{\mathsf{j}x}\big]$ of a Gaussian random variable $x \sim \mathcal{N}(\mu, \sigma^2)$, is given by $\mathbb{E}\big[\mathsf{e}^{\mathsf{j}x}\big] = M_x(\mathsf{j}) = \mathsf{e}^{\mathsf{j}\mu - \frac{\sigma^2}{2}}$ [52]. If $\varphi_{\mathrm{m}} \sim \mathcal{N}(0, \sigma^2_{\mathrm{sw}})$, then $2\varphi_{\mathrm{m}}, -2\varphi_{\mathrm{m}} \sim \mathcal{N}(0, 4\sigma^2_{\mathrm{sw}})$ and $\mathbb{E}[\mathsf{cos}^2(\varphi_{\mathrm{m}})]$ can be calculated as:

$$\mathbb{E}\big[\mathsf{cos}^2(\varphi_{\mathrm{m}})\big] = \frac{1}{2} + \frac{1}{4}\mathbb{E}\big[\mathsf{e}^{\mathsf{j}2\varphi_{\mathrm{m}}}\big] + \frac{1}{4}\mathbb{E}\big[\mathsf{e}^{-\mathsf{j}2\varphi_{\mathrm{m}}}\big] = \frac{1}{2} + \frac{1}{2}\mathsf{e}^{-2\sigma^2_{\mathrm{sw}}}. \tag{28}$$

Following a set of similar steps, it can be easily shown that $\mathbb{E}[\mathsf{cos}(\varphi_{\mathrm{m}})] = \mathsf{e}^{-\sigma^2_{\mathrm{sw}}/2}$.

REFERENCES

[1] G. Vougioukas and A. Bletsas, "DoA estimation of a hidden rf source exploiting simple backscatter radio tags," in *Proc. IEEE Int. Conf. Acoust. Speech Signal Process. (ICASSP)*, Toronto, ON, Canada, Jun. 2021, pp. 4355–4359.

[2] H. Stockman, "Communication by means of reflected power," *Proc. IRE*, pp. 1196–1204, 1948.

[3] *EPC Radio-Frequency Identity Protocols, Class-1 Generation-2 UHF RFID Protocol for Communications at 860 MHZ-960 MHZ.* EPC Global, 2015, version 2.0.1.

[4] R. Sadr *et al.*, "RFID systems using distributed exciter network," Mar. 2013, US Patent 8,395,482 B2. [Online]. Available: https://patents.google.com/patent/US8395482B2/en?oq=US8395482

[5] J. Kimionis, A. Bletsas, and J. N. Sahalos, "Increased range bistatic scatter radio," *IEEE Trans. Commun.*, vol. 62, no. 3, pp. 1091–1104, Mar. 2014.

[6] P. N. Alevizos, K. Tountas, and A. Bletsas, "Multistatic scatter radio sensor networks for extended coverage," *IEEE Trans. Wireless Commun.*, vol. 17, no. 7, pp. 4522–4535, Jul. 2018.

[7] M. Ouroutzoglou, G. Vougioukas, G. N. Karystinos, and A. Bletsas, "Multistatic Noncoherent Linear Complexity Miller Sequence Detection for Gen2 RFID/IoT," *IEEE Trans. Wireless Commun.*, pp. 1–1, Jun. 2021.

[8] G. Vannucci, A. Bletsas, and D. Leigh, "A software-defined radio system for backscatter sensor networks," *IEEE Trans. Wireless Commun.*, vol. 7, no. 6, pp. 2170–2179, Jun. 2008.

[9] A. Bletsas, P. N. Alevizos, and G. Vougioukas, "The art of signal processing in backscatter radio for μW (or less) internet of things: Intelligent signal processing and backscatter radio enabling batteryless connectivity," *IEEE Signal Processing Mag.*, vol. 35, no. 5, pp. 28–40, Sep. 2018.

[10] E. Kampianakis, J. Kimionis, K. Tountas, C. Konstantopoulos, E. Koutroulis, and A. Bletsas, "Wireless environmental sensor networking with analog scatter radio & timer principles," *IEEE Sensors J.*, vol. 14, no. 10, pp. 3365–3376, Oct. 2014.

[11] C. Konstantopoulos, E. Koutroulis, N. Mitianoudis, and A. Bletsas, "Converting a plant to a battery and wireless sensor with scatter radio and ultra-low cost," *IEEE Trans. Instrum. Meas.*, vol. 65, no. 2, pp. 388–398, Feb. 2016.

[12] S. N. Daskalakis, S. D. Assimonis, E. Kampianakis, and A. Bletsas, "Soil moisture scatter radio networking with low power," *IEEE Trans. Microwave Theory Tech.*, vol. 64, no. 7, pp. 2338–2346, Jul. 2016.

[13] S. Thomas, E. Wheeler, J. Teizer, and M. Reynolds, "Quadrature amplitude modulated backscatter in passive and semipassive UHF RFID systems," *IEEE Trans. Microwave Theory Tech.*, vol. 60, no. 4, pp. 1175–1182, Apr. 2012.

[14] N. Fasarakis-Hilliard, P. N. Alevizos, and A. Bletsas, "Coherent detection and channel coding for bistatic scatter radio sensor networking," *IEEE Trans. Commun.*, vol. 63, pp. 1798–1810, May 2015.

[15] J. F. Ensworth and M. S. Reynolds, "Every smart phone is a backscatter reader: Modulated backscatter compatibility with bluetooth 4.0 low energy (BLE) devices," in *Proc. IEEE RFID*, San Diego, CA, Apr. 2015, pp. 78–85.

[16] D. Bharadia, K. R. Joshi, M. Kotaru, and S. Katti, "Backfi: High throughput wifi backscatter," in *Proc. ACM SIGCOMM*, London, United Kingdom, 2015, pp. 283–296.

[17] G. Vougioukas, S. N. Daskalakis, and A. Bletsas, "Could battery-less scatter radio tags achieve 270-meter range?" in *Proc. IEEE Wireless Power Transfer Conf. (WPTC)*, Aveiro, Portugal, May 2016, pp. 1–3.

[18] P. N. Alevizos, A. Bletsas, and G. N. Karystinos, "Noncoherent short packet detection and decoding for scatter radio sensor networking," *IEEE Trans. Commun.*, vol. 65, no. 5, pp. 2128–2140, May 2017.

[19] P. Zhang, D. Bharadia, K. Joshi, and S. Katti, "Hitchhike: Practical backscatter using commodity wifi," in *Proceedings of the 14th ACM Conference on Embedded Network Sensor Systems CD-ROM*, ser. SenSys '16. New York, NY, USA: ACM, 2016, pp. 259–271.

[20] V. Liu, A. Parks, V. Talla, S. Gollakota, D. Wetherall, and J. R. Smith, "Ambient backscatter: Wireless communication out of thin air," in *Proc. ACM SIGCOMM*, Hong Kong, China, 2013, pp. 39–50.

[21] A. Wang, V. Iyer, V. Talla, J. R. Smith, and S. Gollakota, "FM backscatter: Enabling connected cities and smart fabrics," in *USENIX Symp. on Networked Systems Design and Implementation*, Boston, MA, USA, Mar. 2017.

[22] G. Vougioukas and A. Bletsas, "24μW 26m range batteryless backscatter sensors with FM remodulation and selection diversity," in *Proc. IEEE RFID Techn. and Applications (RFID-TA)*, Warsaw, Poland, Sep. 2017.

[23] M. A. Varner, R. Bhattacharjea, and G. D. Durgin, "Perfect pulses for ambient backscatter communication," in *Proc. IEEE RFID*, Phoenix, AZ, USA, May 2017, pp. 13–19.

[24] N. Van Huynh, D. T. Hoang, X. Lu, D. Niyato, P. Wang, and D. In Kim, "Ambient Backscatter Communications: A Contemporary Survey," Dec. 2017. [Online]. Available: https://arxiv.org/abs/1712.04804

[25] N. Kaina, M. Dupre, G. Lerosey, and M. Fink, "Shaping complex microwave fields in reverberating media with binary tunable metasurfaces," *Scientific Reports*, vol. 4, p. 6693, Oct. 2014.

[26] M. Dupré, P. del Hougne, M. Fink, F. Lemoult, and G. Lerosey, "Wave-field shaping in cavities: Waves trapped in a box with controllable boundaries," *Phys. Rev. Lett.*, vol. 115, p. 017701, Jul. 2015.

[27] M. Di Renzo *et al.*, "Smart radio environments empowered by reconfigurable AI meta-surfaces: an idea whose time has come," *EURASIP Journal on Wireless Communications and Networking*, vol. 2019, no. 1, p. 129, May 2019.

[28] E. Basar, M. Di Renzo, J. de Rosny, M. Debbah, M.-S. Alouini, and R. Zhang, "Wireless Communications Through Reconfigurable Intelligent Surfaces," Jun. 2019. [Online]. Available: https://arxiv.org/abs/1906.09490

[29] G. Lerosey *et al.*, "Waveforming device and wave receiver," May 2019, Patent FR3066665B1. [Online]. Available: https://patents.google.com/patent/FR3066665B1

[30] Z. Li, Y. Xie, L. Shangguan, R. I. Zelaya, J. Gummeson, W. Hu, and K. Jamieson, "Towards programming the radio environment with large arrays of inexpensive antennas," in *Proc. USENIX Symp. Netw. Syst. Design Implement.*, Feb. 2019, pp. 285–300.

[31] V. Arun and H. Balakrishnan, "RFocus: Practical beamforming for small devices," 2019. [Online]. Available: http://arxiv.org/abs/1905.05130

[32] G. Vougioukas, A. Bletsas, and J. N. Sahalos, "Instantaneous, zero-feedback fading mitigation with simple backscatter radio tags," *IEEE J. Radio Freq. Identif.*, Oct. 2020, early access.

[33] I. Vardakis, G. Kotridis, S. Peppas, K. Skyvalakis, G. Vougioukas, and A. Bletsas, "Intelligently wireless batteryless RF-powered reconfigurable surface," May 2021. [Online]. Available: https://arxiv.org/abs/2105.14475

[34] W. Tang, J. Y. Dai, M. Z. Chen, K.-K. Wong, X. Li, X. Zhao, S. Jin, Q. Cheng, and T. J. Cui, "MIMO transmission through reconfigurable intelligent surface: System design, analysis, and implementation," *IEEE Trans. Commun.*, vol. 38, no. 11, pp. 2683–2699, Nov. 2020.

[35] P. Chen, Z. Yang, Z. Chen, and Z. Guo, "Reconfigurable intelligent surface aided sparse DOA estimation method with non-ULA," *IEEE Signal Processing Letters*, vol. 28, pp. 2023–2027, Sep. 2021.

[36] T. Ohira and K. Iigusa, "Electronically steerable parasitic array radiator antenna," *Electronics and Communications in Japan (Part II: Electronics)*, vol. 87, no. 10, pp. 25–45, 2004.

[37] A. Kalis, A. G. Kanatas, and C. B. Papadias, "A novel approach to mimo transmission using a single rf front end," *IEEE J. Select. Areas Commun.*, vol. 26, no. 6, pp. 972–980, Aug. 2008.

[38] A. Kalis, A. Kanatas, and C. Papadias, *Parasitic Antenna Arrays for Wireless MIMO Systems*. Springer, 2013.

[39] C. Sun, A. Hirata, T. Ohira, and N. C. Karmakar, "Fast beamforming of electronically steerable parasitic array radiator antennas: theory and experiment," *IEEE Trans. Antennas Propagat.*, vol. 52, no. 7, pp. 1819–1832, Jul. 2004.

[40] A. Li, C. Masouros, and C. B. Papadias, "MIMO transmission for single-fed espar with quantized loads," *IEEE Trans. Commun.*, vol. 65, no. 7, pp. 2863–2876, Apr. 2017.

[41] Z. Han, Y. Zhang, S. Shen, Y. Li, C.-Y. Chiu, and R. Murch, "Characteristic mode analysis of ESPAR for single-RF MIMO systems," *IEEE Trans. Wireless Commun.*, vol. 20, no. 4, pp. 2353–2367, Dec. 2021.

[42] J. Lee, J. Y. Lee, and Y. H. Lee, "Spatial multiplexing of ofdm signals with qpsk modulation over espar," *IEEE Trans. Veh. Technol.*, vol. 66, no. 6, pp. 4914–4923, Oct. 2017.

[43] C. Plapous, J. Cheng, E. Taillefer, A. Hirata, and T. Ohira, "Reactance domain music algorithm for electronically steerable parasitic array radiator," *IEEE Trans. Antennas Propagat.*, vol. 52, no. 12, pp. 3257–3264, Dec. 2004.

[44] P. Nikitin, "Self-reconfigurable rfid reader antenna," in *Proc. IEEE RFID*, Phoenix, AZ, May 2017, pp. 88–95.

[45] G. Vougioukas, "Scatter radio relaying and applications," Ph.D. dissertation, School of ECE, Technical University of Crete, Chania, Greece, 2020, advisor: A. Bletsas.

[46] S. M. Kay, *Fundamentals of statistical signal processing. [Volume I]. , Estimation theory*. Upper Saddle River (N.J.): Prentice Hall, 1993.

[47] J. G. Proakis and M. Salehi, *Communication Systems Engineering*, 2nd ed. Upper Saddle River, NJ, USA: Prentice-Hall, 2001.

[48] A. Bletsas, A. G. Dimitriou, and J. N. Sahalos, "Improving backscatter radio tag efficiency," *IEEE Trans. Microwave Theory Tech.*, vol. 58, no. 6, pp. 1502–1509, Jun. 2010.

[49] G. Vougioukas and A. Bletsas, "Switching frequency techniques for universal ambient backscatter networking," *IEEE J. Select. Areas Commun.*, vol. 37, no. 2, pp. 464–477, Feb. 2019.

[50] R. Schmidt, "Multiple emitter location and signal parameter estimation," *IEEE Trans. Antennas Propagat.*, vol. 34, no. 3, pp. 276–280, Mar. 1986.

[51] A. Goldsmith, *Wireless Communications*. New York, NY, USA: Cambridge University Press, 2005.

[52] F. Oberhettinger, *Fourier Transforms of Distributions and Their Inverses: A Collection of Tables*, ser. Probability & Mathematical Statistics Monograph. Academic Press, 1973.